Title

Parametric Study for Miniaturized Tensile Testing of HDPE for Application in Astronaut Crew Mobility, Infrastructure, and Refabricated Devices

Author

Pastrnak, Austin

Publication Date

2019

Peer reviewed|Thesis/dissertation

Parametric Study for Miniaturized Tensile Testing of HDPE for Application in Astronaut Crew Mobility, Infrastructure, and Refabricated Devices

By

AUSTIN JOHN PASTRNAK

THESIS

Submitted in partial satisfaction of the requirements for the degree of

MASTER OF SCIENCE

in

Mechanical and Aerospace Engineering

in the

OFFICE OF GRADUATE STUDIES

of the

UNIVERSITY OF CALIFORNIA

DAVIS

Approved:

_____

Dr. Valeria La Saponara, Chair

_____

Dr. Mark Rashid

_____

Dr. Sabbie Miller

Committee in Charge

2019

To my friends and family

ACKNOWLEDGMENTS

I would like to thank Dr. Valeria La Saponara for serving as my thesis advisor and providing imperative guidance towards completing my research. I would also like to thank Dr. Mark Rashid and Dr. Sabbie Miller for serving as my thesis committee members. Special thanks to Dr. Miller for also kindly granting me access to her testing equipment and laboratory. I am truly grateful for the research assistance of ACRES laboratory member, Adriana Henriquez, along with support from ACRES member Shreya Rastogi and Andy Cobb of the BAE machine shop. I acknowledge funding for my thesis work by NASA Solar System Exploration Research Virtual Institute, agreement #NNA17BF68A.

Furthermore, I am incredibly thankful for my mother and father, Bonnie and John Pastrnak, who have provided tremendous support throughout my life. Lastly, I would like to acknowledge two of my dear friends, Alicia Diebner and Robert Ferris, who have accompanied me along my journey through engineering at UC Davis and have made many great memories along the way.

Austin Pastrnak

CONTENTS

List of Figures

List of Tables

Acronyms and Abbreviations

ASTM..... American Society for Testing and Materials
ACRES..... Advanced Composites Research, Engineering, and Science
BAE ..... Biological and Agricultural Engineering
CAL..... Calibration
DAQ.....Data Acquisition Unit
DOD..... Department of Defense
HDPE .....High Density Polyethylene
HYS .....Hysteresis
ISS ..... International Space Station
LIN .....Linearity
MCM..... Monte Carlo Method
MTS ..... Material Testing System
NASA.....National Aeronautics and Space Administration
PLA..... Polyactic Acid
REP.....Reproducibility
RES.....Resolution
SSERVI ..... Solar System Exploration Research Virtual Institute

ABSTRACT

The tensile properties of nano-structured materials are often measured by small-scale samples. Specimens may deviate from the sizes and geometries dictated by conventional testing standards, such as ASTM International. The parametric study of this thesis examines the scaling effects present when altering the dimensions of uniaxial tensile test specimens of high-density polyethylene (HDPE); a thermoplastic polymer that is recyclable, can be 3D-printed, and has a wide range of engineering applications, from pipes, to toys, and bottles. Moreover, polyethylene has also a long track record of radiation protection shielding and is being considered for manned space missions beyond the protection of Earth's magnetic field. In this thesis, the variation of mechanical properties from ASTM D638 Types I-IV for reinforced and unreinforced plastics, to ASTM D3039 typically used for fiber-reinforced composites are studied. These were water-jet machined and tested on a hydraulic machine. A Monte Carlo method for uncertainty estimation was adopted for the probability distribution of maximum stress at the yield point. Furthermore, the stress-strain behaviors are fitted to an empirical model, used in conjunction with finite element analysis, with the goal of predicting the material response of the tensile test results of several standardized geometries. This project is a useful tool for modeling HDPE's material response across a range of applications and could be extended to other polymers.

CHAPTER 1

INTRODUCTION AND LITERATURE REVIEW

The work discussed in this Chapter is extracted from the pre-peer reviewed version of a journal paper submitted on September 28th, 2019 to an archival journal. The paper is authored by myself, Adriana Henriquez and Valeria La Saponara, and has title "Parametric Study for Miniaturized Tensile Testing of HDPE for Application in Crew Mobility, Infrastructure and Refabricated Devices". I am the main author of this journal paper.

1.1 Motivation

High-density polyethylene (HDPE) is a thermoplastic polymer that can be 3D-printed, recycled, and has a broad range of applications in food containers, corrosion-resistant pipes, toys, decking material, etc. It also has documented resistance to radiation due to its high hydrogen content (Dougherty and Adams, 1983; Kreiger et al., 2014; Narici et al., 2017). HDPE can be 3D-printed in space and alleviate the need for custom tooling and manufacturing on human habitats such as the International Space Station (ISS), meeting a number of NASA recent initiatives ("Refabricator" for recycling 3D-printable polymers, as discussed by Prater et al., (2017), "In Space Resource Utilization" and "In Space Additive Manufacturing" to

print tools/parts, possibly incorporating regolith, "Centennial challenge: 3D-printed habitat challenge"). Such a development could enable fabrication of 3D-printed structures not constrained by launch requirements, and decrease both the mass of spares onboard, and the mass requirements for building up infrastructure. It is also possible to incorporate properly functionalized inorganic particles into HDPE in order to improve the material's mechanical properties while retaining the radiation resistance. For example, Harrison et al. (2008) used surface functionalization to adhere boron nitride with polyethylene, resulting in a 25% increase in tensile modulus for 15 vol % filler, along with improved radiation shielding measurements.

1.2 Importance of Electrical Conductivity

Within space applications, HDPE treated with nanomaterials such as graphene can be adopted to obtain a multifunctional composite structure: a radiation-resistant, electrically conductive material with a range of mechanical, thermal and electrical properties that can be adapted to spacesuits, crew surface mobility, and human habitats (Laurenzi et al., 2018; Orlando et al., 2018; Seibers et al., 2019). A spacesuit is comparable to a personal spaceship in that it provides thermal regulation and basic protection while allowing an astronaut to explore the harsh space environment, which includes facing differential charging issues. In the terrestrial magnetosphere, charging anomalies have been observed when a spacecraft is flying through the hot terrestrial plasma sheet or large current flows of the geomagnetic tail, where negative 10kV potentials have been reported by a spacecraft (Farrell et

al., 2015). Given these conditions, it is common practice to require the skin of a spacecraft to have strict conductivity requirements, to mitigate electric charging issues. Researchers believe that these requirements should extend to spacesuits as well, given that they are also exposed to the space plasma environment (Farrell et al., 2015). An astronaut moving over the lunar surface creates a tribo-electric charge, and since the Moon is a poor conductor, the astronaut would be grounded to the free reservoir of charge in the local plasma and not to the lunar surface. A material such as an HDPE-based nanocomposite could meet the electrical conductivity requirement while also acting as an effective radiation shield. The electrical conductivity property also allows for structural health monitoring techniques, such as electrical resistance tomography, therefore the material could be in principle self-sensing its own radiation and/or mechanical damage, similarly to what was done in prior work (Lestari et al., 2016; Clausi et al., 2019). For NASA 3D-printed habitats for sustainable housing in deep space exploration missions, one could envision the use of reinforced, multifunctional HDPE panels. This endeavor and its scale will require careful tailoring of mechanical properties.

1.3 The Need to Scale-Up

According to the U.S. Department of Defense Composite Materials Handbook (MIL-HDBK-17-3F, section 4.4.2.1), the U.S. Department of Defense (DOD) and NASA need to generate static strength and stiffness properties of polymer matrix composites utilizing ASTM D3039 (for tensile properties, the focus of this paper),

D3410 (for compressive properties), and D3518 (for in-plane shear properties), for engineering and manufacturing development and production of aircraft. Strengthening of civil structures with fiber-reinforced polymer composites requires the measurement of material properties with ASTM D3039 (as indicated in ASTM D7565). ASTM requires the use of D3039 for reinforced polymer composites with continuous or discontinuous high-modulus fibers having a Young's modulus larger than 20 GPa, consistently with the structural needs of aircraft and civil infrastructure. However, limited resources (for example, access to raw materials in space) may drive the manufacturing of smaller test samples for mechanical properties, such as those encompassed by Types I-IV samples in ASTM D638, the standard for reinforced and unreinforced polymers of lower modulus. These design considerations drive the applied research question behind this thesis: how a material's stress-strain response changes as the material's size is scaled-up from (for example) a small tool size to the size used for human habitats, and which of the D638 geometries yield the most statistically similar properties to those obtained from testing the DOD and NASA approved D3039 standard geometry of the same material.

1.4 Known Material Response

1.4.1 Material Necking

When loaded in tension, many polymers develop necking after the load-elongation curve reaches a maximum yield point and then the deformed area localizes

under decreasing load. This elongation is accomplished primarily by a propagation of the neck boundaries along the specimen in a process termed "cold drawing" by Carothers and Hill (1932), which is of practical interest as the polymer transitions to a stiffer and harder state. This was initially published by Considère (1885). Three concepts provide the framework for understanding neck formation. All real materials have flaws or local variations in dimensions which cause local fluctuations in stresses and strains. During tensile deformation, the material decreases in cross-sectional area and strain hardens. The amount of hardening varies with the extent of deformation. The location of stress fluctuations determines the location of the neck, and the strain hardening rate determines the neck's stability. Fig. 1 shows the construction of Hutchinson and Neale's (1983) empirical equations of tensile response (Eq. 1A – 1B), with Considère's criterion showing the tangent lines corresponding to neck initiation (A) and neck stabilization (B). The symbol k is a material constant and λ is termed the "stretch ratio".

$$\sigma_t = k\alpha\varepsilon_t^b \; ; \; \varepsilon_t < \varepsilon_0 \tag{1A}$$

$$\sigma_t = k\exp(c\varepsilon_t^2) \; ; \; \varepsilon_t \geq \varepsilon_0 \tag{1B}$$

In Eq. 1A – 1B, the variables α, b, c, and ε_0 are related by continuity of true stress σ_t and its first derivative with respect to strain at $\varepsilon_t = \varepsilon_0$.

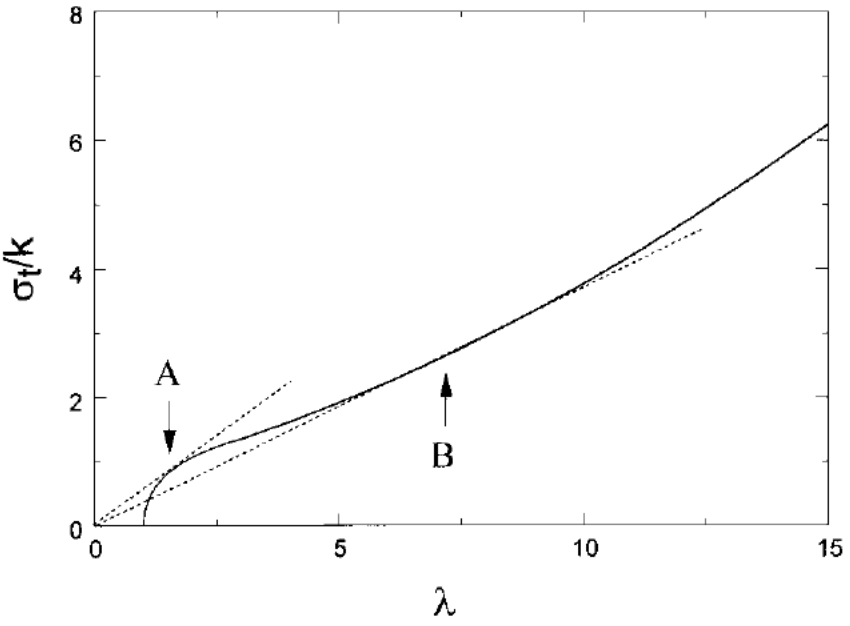

Fig. 1: Considère construction for neck formation and stabilization. (Crist, B., and Metaxas, C., 2003).

Steady-state neck propagation has since been analyzed by Coleman (1983) within the one-dimensional equilibrium theory of bars. Hutchinson and Neale (1983) have expanded this to an approximate three-dimensional analysis for axisymmetric neck propagation along cylindrical round bars. Neale and Tugcu (1985) have then carried out a full three-dimensional finite element analysis for the entire load-deformation behavior of a round tensile specimen.

1.4.2 Hyperelasticity

The current paper's work is focused only on the material's elastic properties and the stress-strain response before necking occurs (below 20% strain) to examine

the maximum stress experienced by the material in its initial state. Multiple phenomenological models are commonly used to describe the observed hyperelastic behavior. The polynomial hyperelastic model was introduced by Rivlin and Saunders (1951). It was formulated in terms of the two strain invariants $\bar{I}_1$ and $\bar{I}_2$ of the left Cauchy-Green deformation tensor. C_{ij} denote material constants. The material's strain energy W is given by Eq. 2. This model is adapted to include and volume dependence which is used in Section 3.6 of this thesis to generate the hyperelastic behavior of uniaxial tensile testing modeled in finite element analysis (FEA).

$$W = \sum_{i=j=0}^{n} C_{ij}(\bar{I}_1 - 3)^i(\bar{I}_2 - 3)^j \tag{2}$$

The Ogden model (Ogden, 1972) (Eq. 3) expresses the strain energy function W in terms of principal stretches λ_1, λ_2, and λ_3, where μ_p and α_p are material constants. This model matches well to experimental evidence at stretches where crystallization is not significant (Ogden, 1972).

$$W = \sum_{p=1}^{n} \frac{\mu_p}{\alpha_p}(\lambda_1{}^{\alpha_p} + \lambda_2{}^{\alpha_p} + \lambda_3{}^{\alpha_p} - 3) \tag{3}$$

Furthermore, Yeoh (1993) developed a hyperelastic model that only depends on the first strain invariant. The original model shows the series truncated after the first three terms, and Selvadurai (2006) introduced a more general definition of the strain energy (Eq. 4).

$$W = \sum_{i=1}^{n} C_i(\bar{I}_1 - 3)^i \tag{4}$$

HDPE specifically has a wide range of material properties that are functions of various testing parameters such as strain rate and temperature (Milisavljevic et al., 2012), so this study aims to keep those variables fixed as much as possible, and only examine geometric effects under those conditions, as discussed further on.

CHAPTER 2

EXPERIMENTAL PROCEDURE

The work discussed in this Chapter is extracted from the pre-peer reviewed version of a journal paper submitted on September 28th, 2019 to an archival journal. The paper is authored by myself, Adriana Henriquez and Valeria La Saponara, and has title "Parametric Study for Miniaturized Tensile Testing of HDPE for Application in Crew Mobility, Infrastructure and Refabricated Devices". I am the main author of this journal paper.

2.1 Test Sample Design and Preparation

Full density sheets of molded HDPE were obtained from McMaster-Carr with stock thickness of 2.38 mm (3/32") that follow ASTM D4976, the standard specification for polyethylene plastics. Details such as the purity, molecular weight, and polymer chain length are important variables in HDPE, but this information was not provided by McMaster-Carr. Dog-bone tensile samples were cut out using numerically controlled water-jet machining. These samples followed the lateral dimensions shown in Fig. 2 – 6. These are composed of ASTM D638 Types I, II, III, and IV, as well as ASTM D3039 for balanced and symmetric geometry (ASTM Standard D638, 2014; ASTM Standard D3039, 2017). The datum marked "A" in these

figures denotes the distance between the testing machine's grips. Due to limitations of the machine's geometry, the actual distance between grips on ASTM D638-III and D3039 was 200mm. All samples conform to the stock thickness of 2.38 mm and the surface finish was not modified, although the edges were deburred of residual polymer strands from machining.

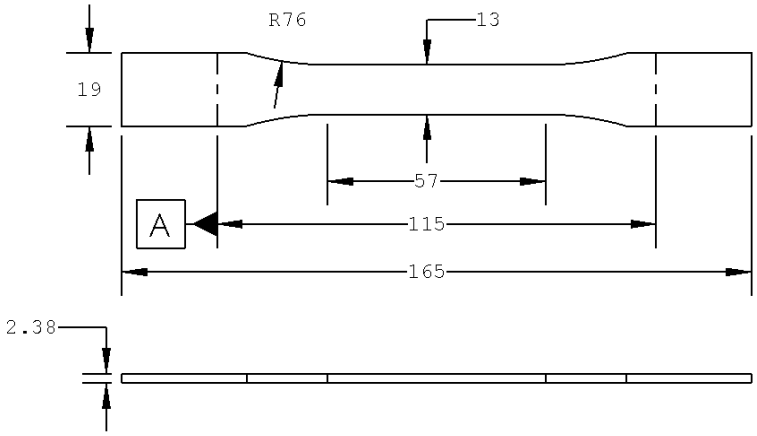

Fig. 2: ASTM D638-I Nominal dimensions (mm).

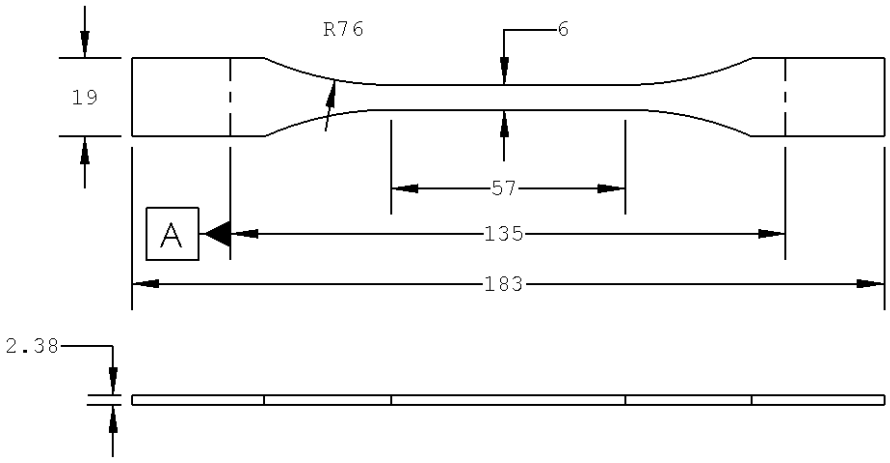

Fig. 3: ASTM D638-II Nominal dimensions (mm).

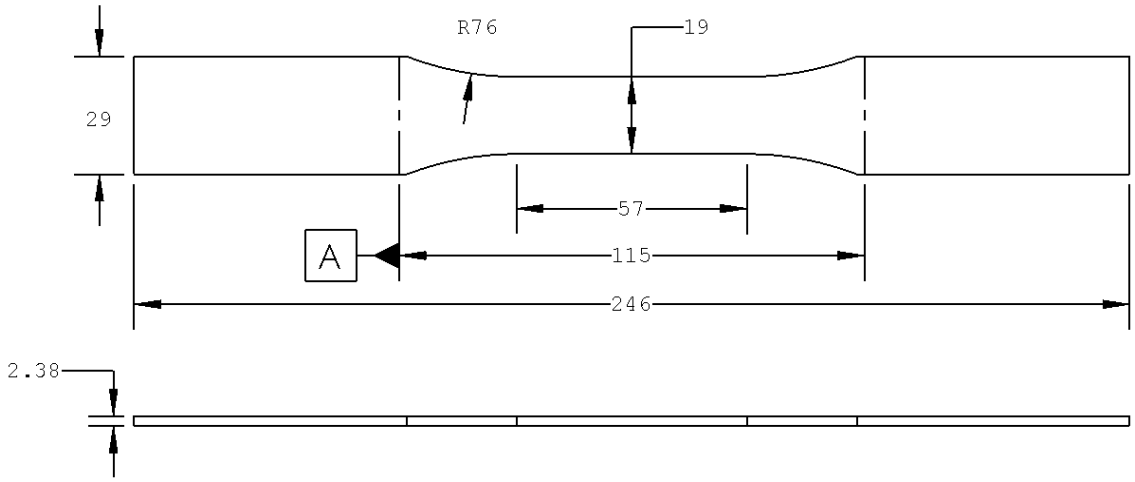

Fig. 4: ASTM D638-III Nominal dimensions (mm).

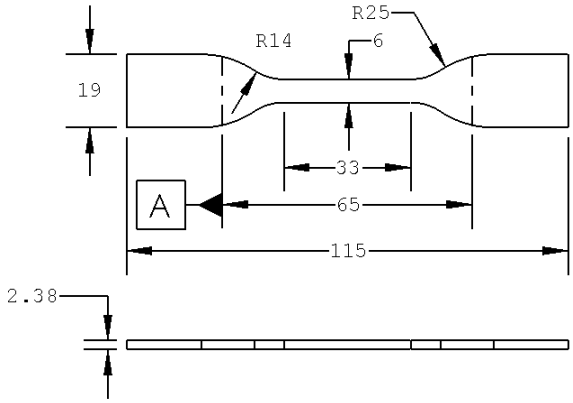

Fig. 5: ASTM-IV Nominal dimensions (mm).

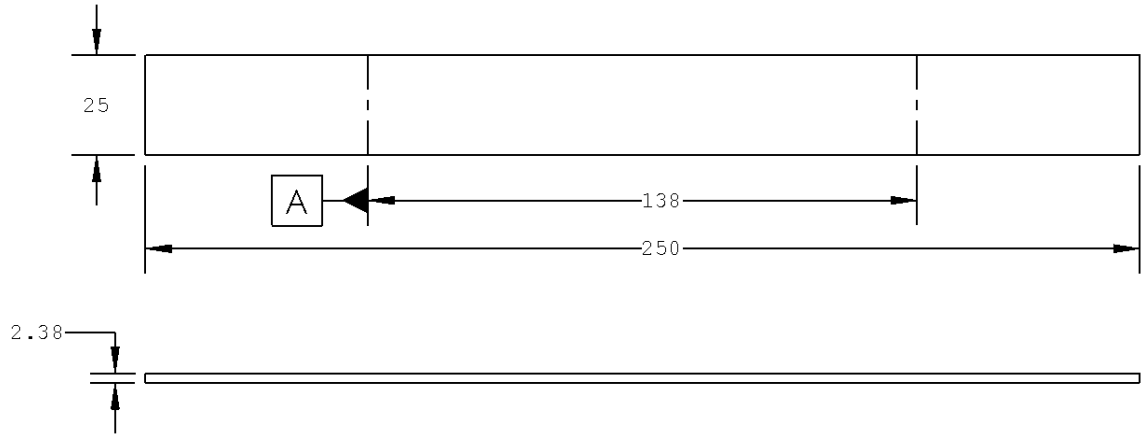

Fig. 6: ASTM D3039 Nominal dimensions for balanced and symmetric orientation (mm).

There were 10 samples tested of each form-factor. Before testing, each sample was measured in three different locations in the gauge length for thickness and width. The average values were reported as the sample's gauge thickness and width, which were used as input parameters for subsequent stress calculations. The as-machined gauge widths of the ASTM D638 samples fell within the tolerances specified (ASTM D638, 2014), while the ASTM D3039 samples exceeded the nominal standard (ASTM D3039, 2017). The quasi-static tensile properties were tested at ambient conditions using a 15kN servo-hydraulic MTS load frame manufactured by MTS (Fig. 7) in displacement control mode that recorded 10 data points per second. The displacement control was set to mimic strain control, which was set to 0.1 mm/mm*/min, where mm* is the length of the narrow section of the test specimen (Table 2). Direct strain control was not used because an instability in the extensometer reading (slip or max readout) could cause the feedback control on the MTS to behave erratically.

Table 1
As-machined test sample gauge widths.

Designation	ASTM Gauge Width (mm)	Measured Gauge Width (mm)
D638-I	12.5 – 13.5	12.75 – 12.89
D638-II	5.5 – 6.5	6.39 – 6.46
D638-III	18.5 – 19.5	19.03 – 19.17
D638-IV	5.5 – 6.5	6.35 – 6.46
D3039	24.75 – 25.25	25.36 – 25.44

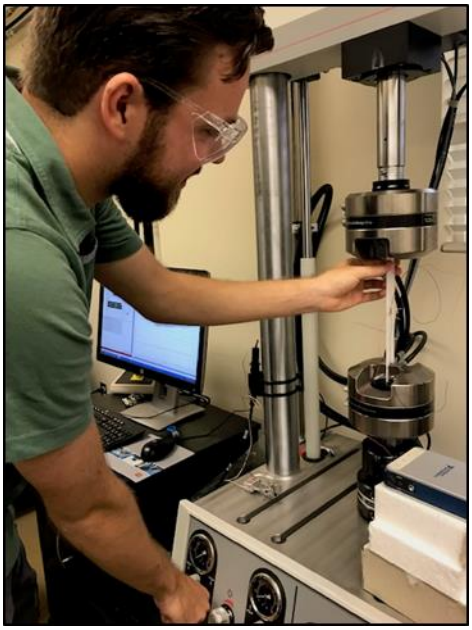

Fig. 7: The thesis' author working on the 15kN load frame.

Table 2
Tensile testing displacement rates.

Designation	Length of Narrow Section (mm)	Displacement Rate (mm/min)
D638-I	57	5.7
D638-II	57	5.7
D638-III	57	5.7
D638-IV	33	3.3
D3039	200	20.0

The strain was recorded using a 25.4 mm gauge length extensometer that interfaced and synchronized with the MTS software. This extensometer is limited 56% strain and was removed from each sample right before that point. This was not a concern because this parametric study does not consider elongations at that level of strain. This extensometer was used for all measurements for consistency. The range of strains of interest are able to be examined with this small-sized extensometer, but

repeating measurements on the larger samples with a larger extensometer would be useful for verification.

For D3039, the length of the narrow section is assumed to be the distance between the grips on the hydraulic machine. No tabs were needed since the material is homogeneous and not unidirectionally dominated. A photographic example of selected pristine and permanently deformed tensile test samples is shown in Fig. 8. The lighter colored regions near the center of the gauge length display stress whitening, which is suggested to be the result of an extensive formation of internal voids (Jareki and Meier, 1979).

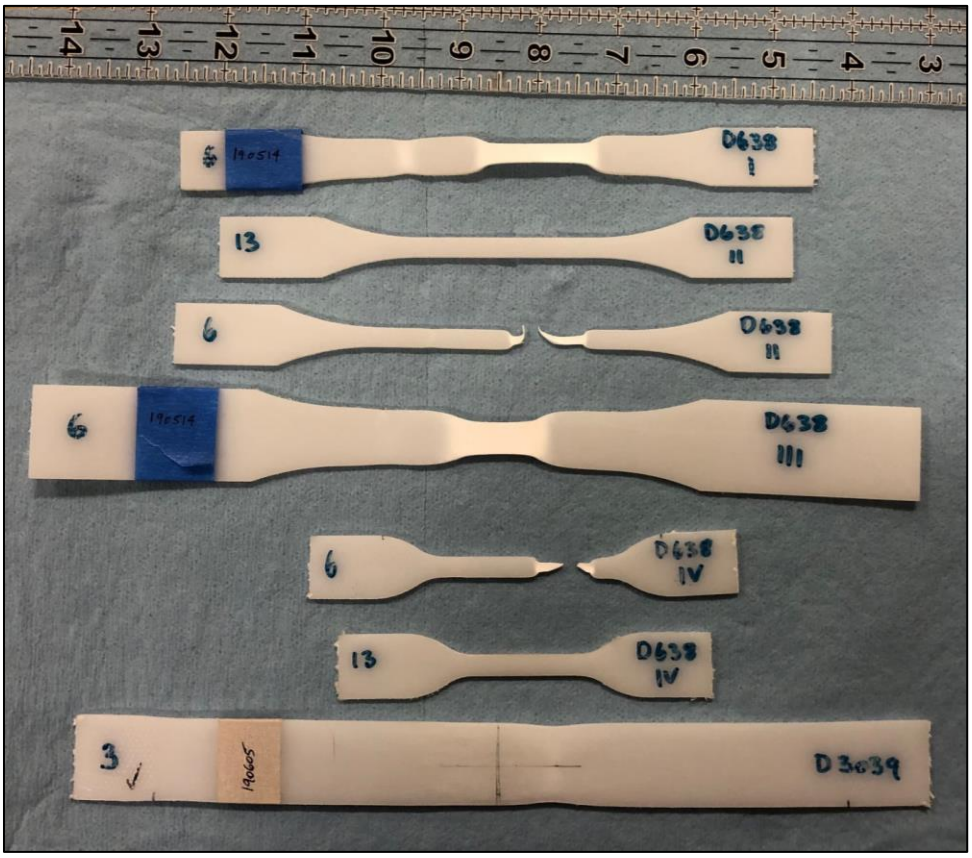

Fig. 8: Photo of ASTM D638 types I-IV and D3039 samples. Two pristine samples (Type II and Type IV) plus samples displaying permanent localized necking, or tensile failure after tensile testing past 20% strain.

2.2 Strain Gauge Setup

Additionally, there was an effort to measure the material's strain with strain gauges complementary to an extensometer. The strain gauges were interfaced with a data acquisition unit (DAQ) and acquired the signal with a LabVIEW program written for a quarter bridge type I configuration at a maximum software-limited rate of 2 samples per second. There was one strain gauge on the longitudinal axis and one on the lateral axis to provide data on Poisson's ratio, which was calculated using Eq. 5. Since there are two active strain elements, a half bridge type I was also examined, but this setup in the software desired a known Poisson's ratio to correct for the Poisson effect. It was not clear that one could acquire two raw data signals (one for each gauge), which was a straightforward process using two quarter bridge type I configurations and necessary to compute Poisson's ratio. Since each strain gauge has some amount of offset from zero, the slopes in lateral and longitudinal measurements were compared rather than the absolute measurements.

$$\upsilon = \left| \frac{\frac{\Delta \varepsilon_{lateral}}{\Delta t}}{\frac{\Delta \varepsilon_{longitudinal}}{\Delta t}} \right| = \left| \frac{\Delta \varepsilon_{lateral}}{\Delta \varepsilon_{longitudinal}} \right| \tag{5}$$

Strain gauges were adhered to the test samples using standard procedures in the ACRES laboratory. The surface was prepared with an acidic compound (Micro Measurements M-Prep Conditioner A) followed by a neutralizer (Micro Measurements M-Prep Neutralizer 5A), then sanded with 100 and 400-grit sandpaper before being cleaned with ethanol. (To clarify, the samples measured with

the extensometer rather than strain gauges did not receive any surface treatment.) Super glue (a cyanoacrylate compound) with a 2-propanol catalyst (Micro Measurements M-Bond Catalyst C) were used. Silver conductive epoxy (MG Chemicals, Type 8331) was used to secure the 30-gauge wires to the solder pads of the strain gauges since the heat from a traditional lead soldering process would melt the HDPE. The epoxy cured overnight before testing at the same strain rate as the extensometer samples: 0.1 mm/mm/min from Table 2.

The problem with strain gauges was that they could only stay adhered to the surface of the HDPE samples for very low strains, particularly for D638-II and D638-IV. These samples had limited width with respect to the size of the strain gauges, and since the tests ran at several millimeters per minute, there was not enough data available to make an accurate assessment throughout the strain regime. This is why an extensometer had to be used for the entire stress-strain curves instead. Data from the Poisson's ratio measurement is presented in Section 3.3.

CHAPTER 3

RESULTS AND DISCUSSION

The work discussed in this Chapter is extracted from the pre-peer reviewed version of a journal paper submitted on September 28th, 2019 to an archival journal. The paper is authored by myself, Adriana Henriquez and Valeria La Saponara, and has title "Parametric Study for Miniaturized Tensile Testing of HDPE for Application in Crew Mobility, Infrastructure and Refabricated Devices". I am the main author of this journal paper.

3.1. Stress-Strain Response of Baseline HDPE

Nominal stress is the instantaneous force F observed by the load cell divided by the average cross-sectional area A along the gauge length of the specimen, and nominal strain is the change in elongation Δl divided by the initial length of the extensometer l_0 (Eq. 6 – 7).

$$\sigma_{nominal} = \frac{F}{A} \tag{6}$$

$$\varepsilon_{nominal} = \frac{\Delta l}{l_0} \tag{7}$$

The stress is assumed to have a uniform distribution across the width of the cross-section. Since the machine was displacement-controlled with respect to time, and the strain was also measured with respect to time, it cannot be assumed that each test undergoes the same strain at the same time, so an index-matching formula was used to take the average of each test's stress result at the closest neighboring strain between tests. These averaged stress-strain results for each geometry are presented in Fig. 9 – 10. Measured values of stress at yield were consistent within a range of 22.5 – 27.0 MPa at a 95% confidence interval, while the accepted range is 23.0 - 29.5 MPa (polymerdatabase.com). These results are presented in Table 3.

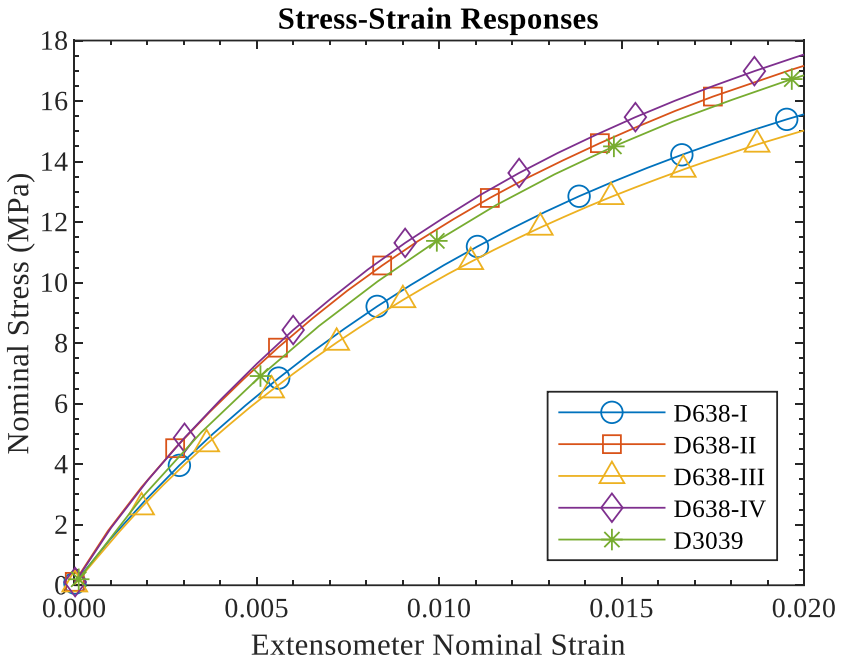

Fig. 9: Average stress-strain curves up to 2% strain.

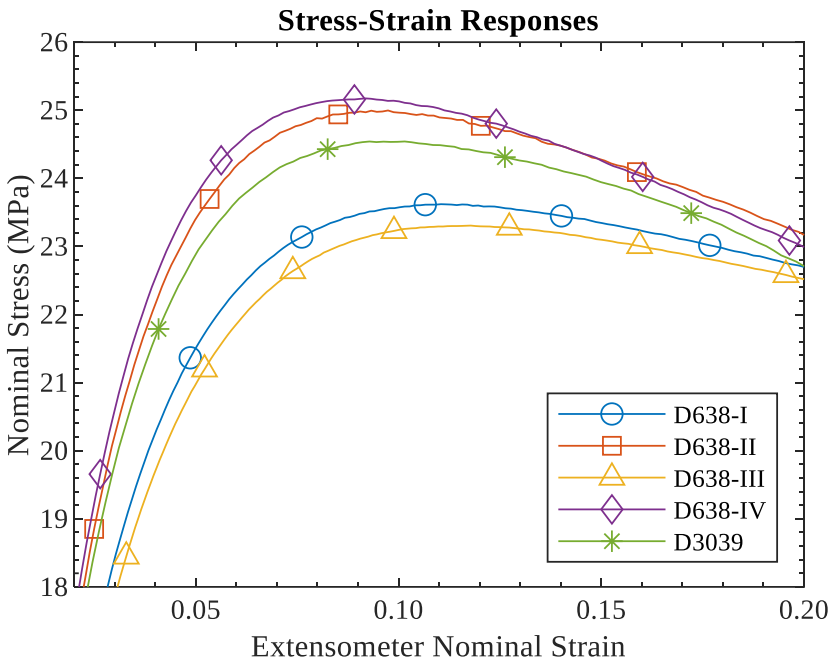

Fig. 10: Average stress-strain curves from 2% up to 20% strain.

In this thesis, the terminology from ASTM D638 is used to define the material behavior. The "yield point" of the material is designated to be the first point on the stress-strain curve at which an increase in strain occurs without an increase in stress. This point is where the material's maximum stress occurs and it is designated the "tensile strength at yield" (ASTM D638, 2014; Kida et al., 2016). This is shown graphically in Fig. 11, where the HDPE similarly resembles the curve that contains points B and C, with the yield point at point B.

This verbiage seems to conflict with the common terminology for metals. The "tensile strength at yield" would classically be called the "ultimate tensile strength." In metals, the word "yield" is used to define a point where further deformation would be plastic deformation (irrecoverable by unloading the material). However, for

polymers, it is often difficult to tell the difference between nonlinear elastic strain and plastic strain before necking. In the necking region, however, the structure of the material changes in an irreversible manner and thus does not recover with unloading. There currently is no known standard that is widely used to make yield stress measurements in polymers, so "yield point" refers to the location of maximum stress, which can be found easily. The most common attempt to measure elastic-plastic transition is to draw a line at a strain offset, with the slope being the elastic modulus and the yield stress would be the intersection of that line and the stress-strain curve. However, several different strain offsets have been used between 0.3% and 2.0%, which give distinctly different results for the yield stress (Semeliss et al, 1990). This thesis does not attempt to establish the transition from elastic-to-plastic strain, and the terminology from ASTM D638 is used instead of common terminology for strength testing metals.

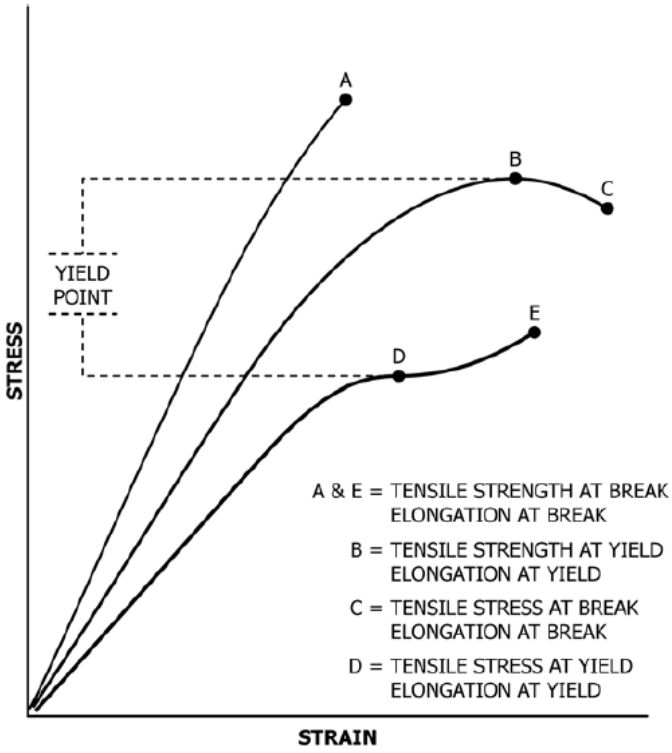

Fig. 11: Graphical definition of yield point for polymers (ASTM D638, 2014).

The stresses and strains at this point for each designation are presented in the box plots in Fig. 12 – 13. On each box, the central mark indicates the median, and the bottom and top edges of the box indicate the 25th and 75th percentile, respectively. The whiskers extend to the most extreme data points not considered outliers, and the outliers are plotted individually using the '+' symbol. A larger scatter in the data was observed for test samples that conform to D638 Type IV, presumably because the magnitude of variations in loading eccentricity and deviations from nominal size are further amplified when evaluating the results at smaller geometries. ASTM D638 Type II is identified as yielding the most

statistically similar stress results as D3039. It could also be suggested that D638 Types I and III are conservative estimates for strength-based design.

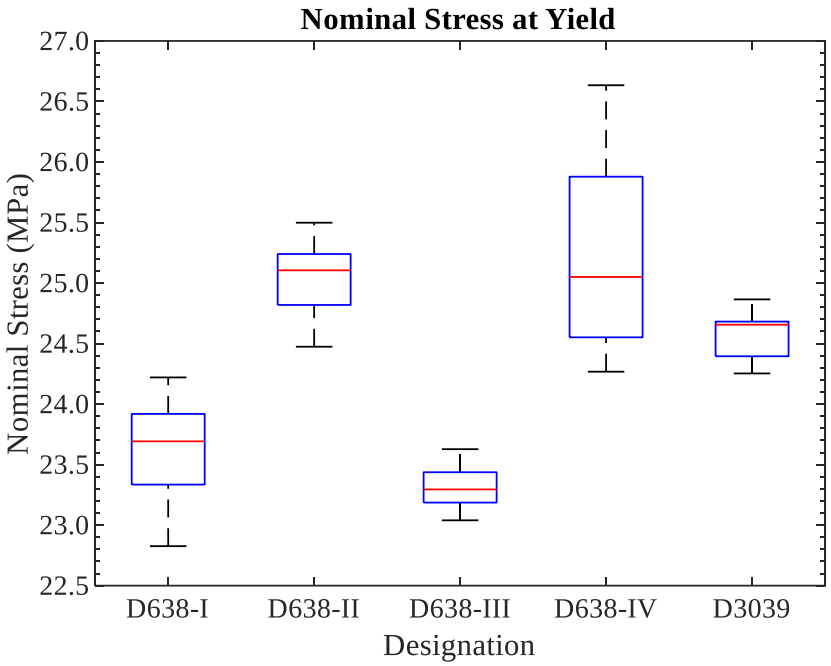

Fig. 12: Boxplot of nominal stresses at yield point.

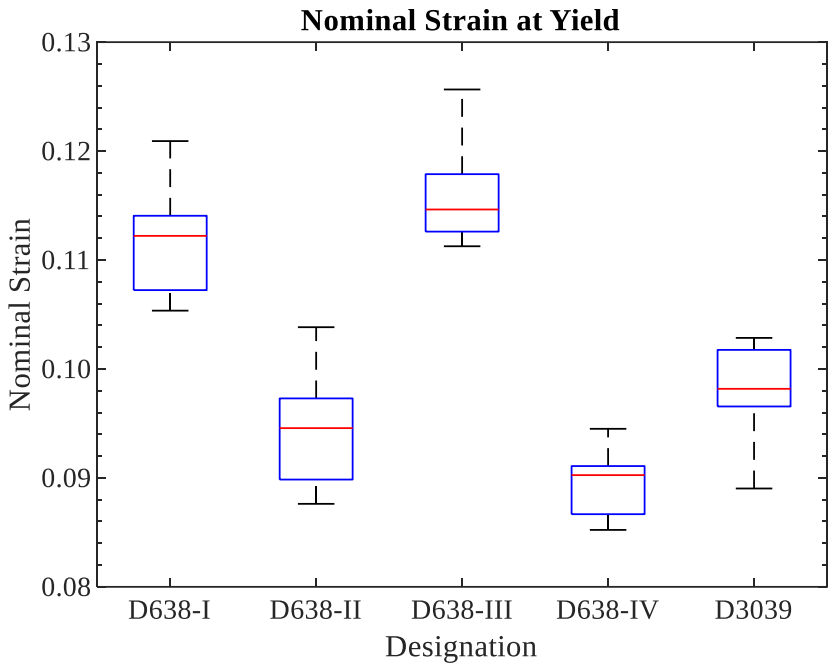

Fig. 13: Boxplot of nominal strains at yield point.

Table 3
Measured mechanical properties of baseline HDPE.

Designation	Stress at Yield (MPa)	Strain at Yield	Elastic Modulus (MPa)
D638-I	22.8 – 24.2	0.105 – 0.121	1204 – 1421
D638-II	24.5 – 25.5	0.087 – 0.104	1433 – 1633
D638-III	23.0 – 23.6	0.111 – 0.126	1195 – 1364
D638-IV	24.3 – 26.6	0.085 – 0.095	1495 – 1638
D3039	24.3 – 24.9	0.089 – 0.103	1335 – 1591
Accepted Value*	23.0 – 29.5	0.090 – 0.180	900 – 1550

*Accepted values at 23C: polymerdatabase.com

3.2. Elastic Modulus Assessment of Baseline HDPE

The stress-strain relations of many plastics do not conform to Hooke's law throughout the elastic range, so the slope of the tangent to the stress-strain curve at a low stress is usually taken as the modulus of elasticity (ASTM D638, 2014). The existence of a true proportional limit in HDPE is questioned, since it is a characterized by both an instantaneous and noninstantaneous elastic response that are dependent on time and temperature (Daver and Cherry, 1996). With those variables fixed, comparison of the elastic moduli at a fixed strain point is realized. The point between 0.1% and 0.2% strain was chosen for this calculation, since the slope of the stress-strain curve significantly deviated from a line beyond this region. The linear region of each test sample was found to be roughly between 0.1% and 0.2% strain, because the samples sometimes exhibited a "toe" artifact where an increase in slope is seen before the linear region. This results from a take up of slack and alignment or seating of the test sample and is not a material property. A linear trendline was fit to the points within this strain region for each sample (12 data points on D638-I, 11 for D638-II and IV, 16 for D638-III, and 10 for D3039) with 10 trendlines for each geometry (one for each test). The linear trendlines used have coefficients of determination (R^2) values above 99.5%. Some samples exhibited a longer linear region that still was under 99.5% R^2, but the same strain point of 0.1 – 0.2% was consistently used for all geometries. The moduli values were computed using the average original cross-sectional area in the gauge length segment of the specimens, as per ASTM D638, and are presented in Fig. 14.

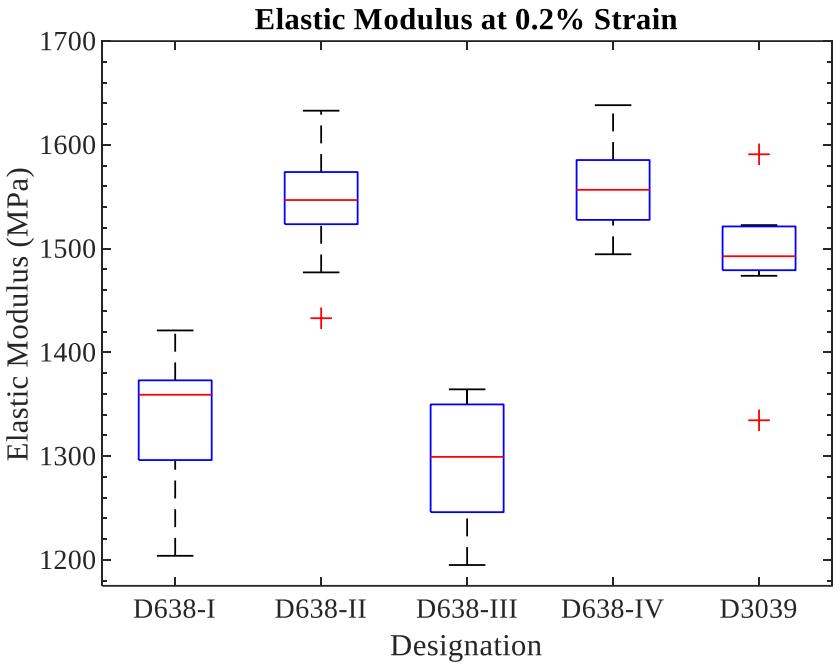

Fig. 14. The measured elastic modulus of each designation.

3.3. Poisson's Ratio Measurement

As mentioned in Chapter 2, two uniaxial strain gauges were used to gather data along the lateral and longitudinal axes of the test samples. This test result is fairly limited in that the gauges did not adhere above low strains, and only the larger form-factor geometries could accommodate a strain gauge along its width. Material constraints limited the tests to only 2 samples of D638-I, D638-III, and D3039. The data from these tests is presented in Table 4. D638-I sample #15 is considered to be an outlier. The overall weighted average Poisson's ratio value of 0.395 was used in subsequent finite element analysis in section 3.6. This value closely agrees with the

commonly accepted range of 0.40 – 0.45, which varies with temperature and strain rate (Nitta and Yamana, 2014).

Table 4.
Poisson's ratio data from two uniaxial strain gauges.

Sample Designation	D638-I #14	D638-I #15	D638-III #14	D638-III #15	D3039 #14	D3039 #15
Median Poisson's Ratio	0.393	0.599	0.393	0.417	0.404	0.367
Average Poisson's Ratio	0.391	0.601	0.392	0.407	0.403	0.367
# of Data Points	40	8	33	34	13	11

3.4. Empirical Model of Stress-Strain Response

Modeling the nominal uniaxial tensile stress-strain responses of the test samples was accomplished in 3 steps of the stress-strain curve. While the material is in its linear elastic region (ε_l), the stress is proportional to nominal strain by Hooke's equation (Eq. 8) where E is the modulus of elasticity.

$$\sigma_{nom} = E\varepsilon_{nom} \tag{8}$$

For nonlinear behavior before yield point/maximum stress (ε_y), a 6th order polynomial is fit to the data (Eq. 9). This region is assumed to be hyperelastic behavior since it occurs well before necking, and a quantifiable transition point

between nonlinear elastic and plastic strain was not established. A polynomial was chosen to fit the data as it has an R2 value above 99.5% for all data points in this region and it has been used to predict this nonlinear elastic behavior in previous literature. Semeliss (1990) used a 5th order polynomial for this region, but a 6th order better satisfies the endpoints of this data. A 7th order polynomial was also examined but provided insignificant advantage. These 6 polynomial constants are presented in Table 5.

$$\sigma_{nom} = a_6{\varepsilon_{nom}}^6 + a_5{\varepsilon_{nom}}^5 + a_4{\varepsilon_{nom}}^4 + a_3{\varepsilon_{nom}}^3 + a_2{\varepsilon_{nom}}^2 + a_1\varepsilon_{nom} + a_0 \quad (9)$$

Finally, for behavior past the yield point, a portion of Hutchinson and Neale's equation modified for stress continuity is used (Eq. 10) (Hutchinson and Neale, 1983).

$$\sigma_{nom} = \alpha k{\varepsilon_{nom}}^N + f \quad (10)$$

All of these model fits are to the data that was averaged in Section 3.1 (Fig. 9 – 10). The linear elastic limit (ε_l) was determined graphically as the point where the slope of the stress-strain data deviates from linear. This was found in Section 3.2 for elastic modulus and 0.002 was used for all samples. The yield point (ε_y) was determined as the average nominal strain corresponding to the peak nominal stress observed during testing. The constants used to model each specimen's behavior in the elastic region and after necking are presented in Tables 5 – 6, and graphical comparisons of the model versus experimental data are presented in Fig. 15 – 19. The models agree within 5% of the experimental data for each geometry presented.

It should be noted that these models can only be said to be valid for this specific strain history since the hyperelastic model may, in reality, include plastic deformation. To be valid for strain histories other than the uniaxial tensile test used to calibrate the model, additional tests would be required to address for how long the material is completely elastic prior to necking. Tests that involve interrupting the loading, and unloading the sample while continuing to take load-displacement data would provide insight to this transition point. A clearer determination of this point and a stress-strain model that encompasses various strain histories can only be had by multiaxial testing.

Table 5
Empirical model parameters for stress-strain response of uniaxial tensile tested HDPE in the linear elastic region and after necking.

Designation	E (MPa)	ε_l	ε_y	α (MPa)	k	N	f (MPa)
D638-I	1331	0.002	0.1118	-2.8	11	2.0	24.0
D638-II	1541	0.002	0.0944	-2.4	25	2.0	25.6
D638-III	1290	0.002	0.1155	-2.0	14	2.0	23.7
D638-IV	1560	0.002	0.0897	-5.1	13	2.0	25.7
D3039	1490	0.002	0.0981	-5.0	11	1.9	25.2

Table 6
Empirical model parameters for 6th order polynomial fit for stress-strain behavior after the linear elastic region, but before necking.

Designation	a_6 (MPa)	a_5 (MPa)	a_4 (MPa)	a_3 (MPa)	a_2 (MPa)	a_1 (MPa)	a_0 (MPa)
D638-I	-1.4654E+8	5.9660E+7	-9.8316E+6	8.5166E+5	-4.2916E+4	1.3360E+3	6.1480E-1
D638-II	-3.6499E+8	1.2487E+8	-1.7336E+7	1.2735E+6	-5.5359E+4	1.5368E+3	8.2171E-1
D638-III	-1.2081E+8	5.0467E+7	-8.5275E+6	7.5674E+5	-3.9079E+4	1.2542E+3	7.5984E-1
D638-IV	-3.8028E+8	1.2723E+8	-1.7369E+7	1.2640E+6	-5.5006E+4	1.5391E+3	1.0601E+0
D3039	-2.9243E+8	1.0606E+8	-1.5614E+7	1.2127E+6	-5.5079E+4	1.5540E+3	2.9852E-1

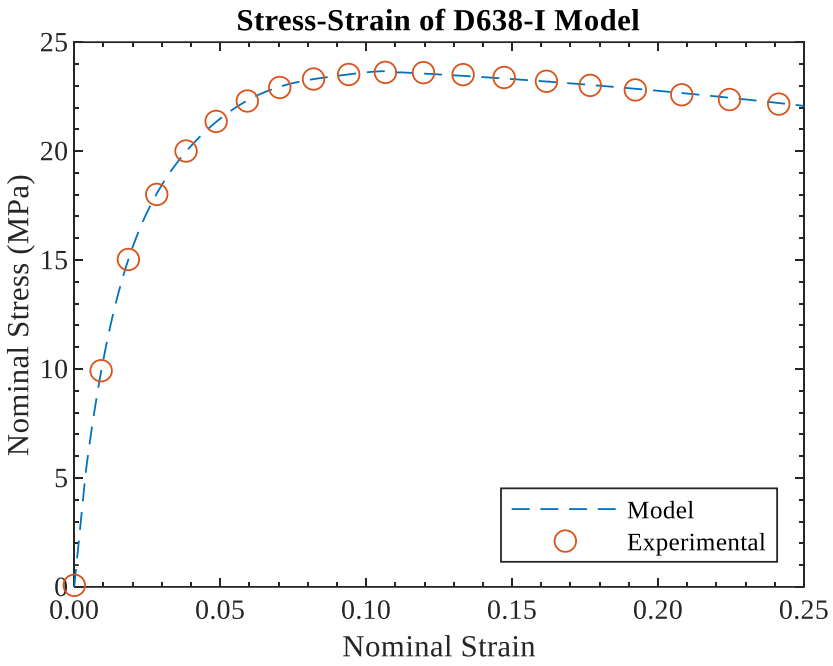

Fig. 15: The empirical stress-strain response model for D638-I.

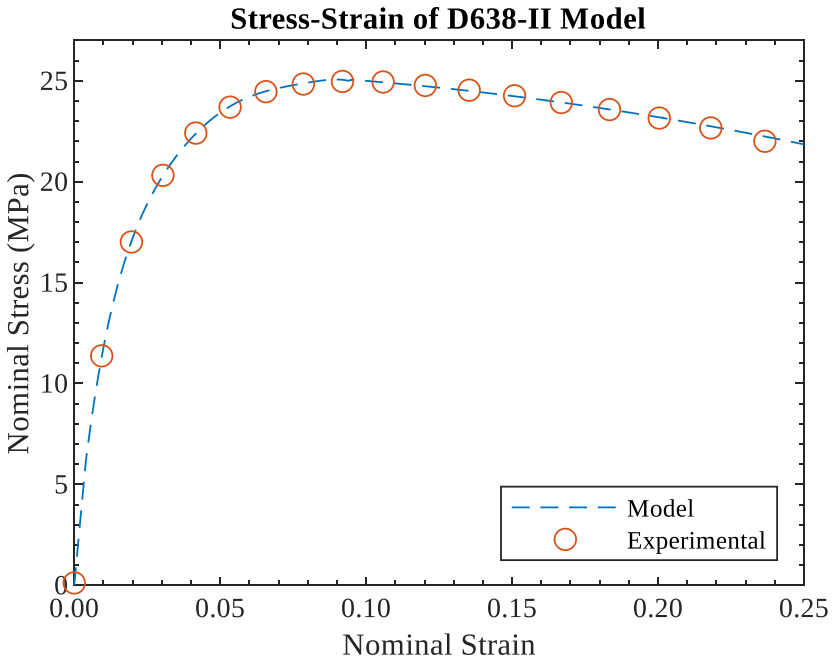

Fig. 16: The empirical stress-strain response model for D638-II.

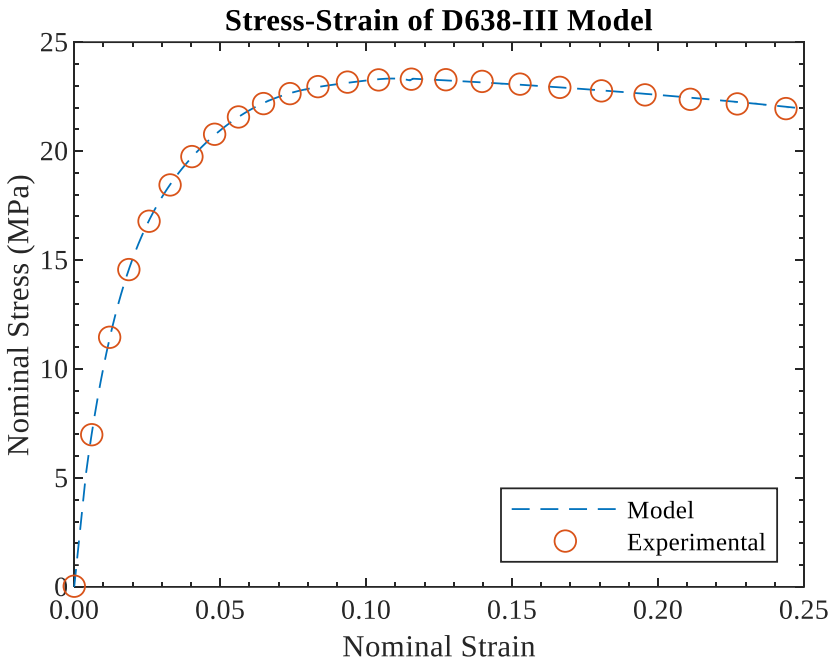

Fig. 17: The empirical stress-strain response model for D638-III.

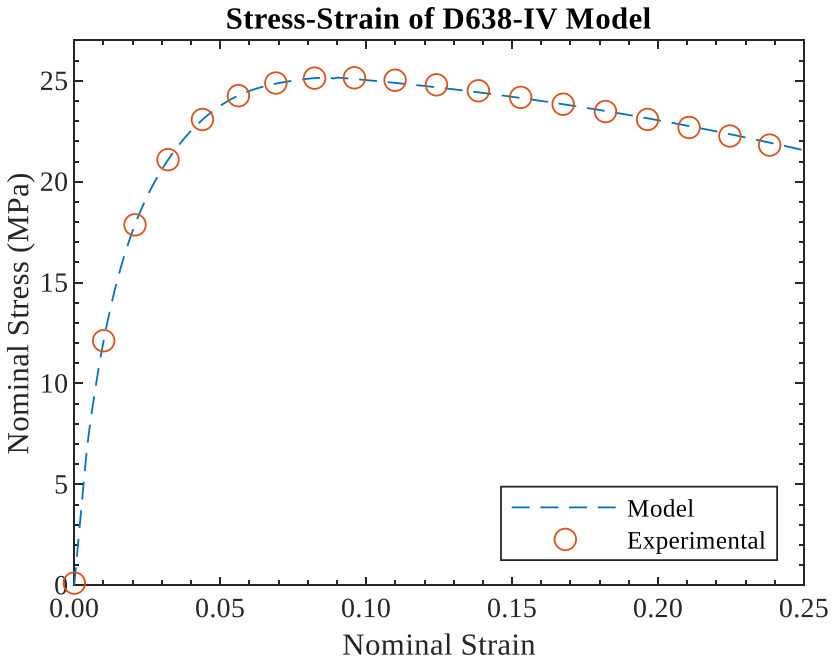

Fig. 18: The empirical stress-strain response model for D638-IV.

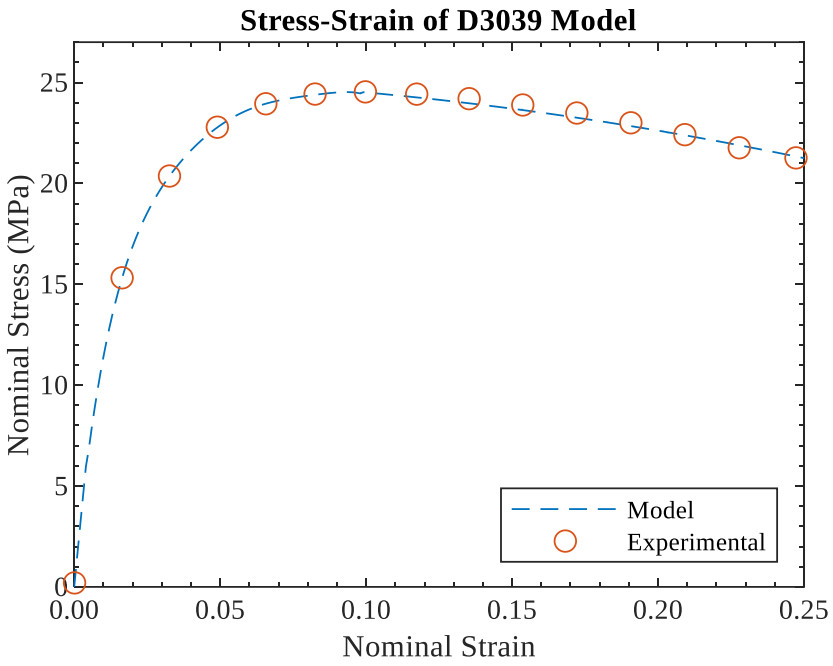

Fig. 19: The empirical stress-strain response model for D3039.

3.5. Propagation of Mechanical Properties by a Monte Carlo Method

A Monte Carlo method (MCM) was used to estimate the uncertainty in the tensile stress calculation for these samples. The Monte Carlo approach provides a means for simulating the stochastic nature of error and their influences on experimental and calculated results (Coleman and Steele, 2009; Joint Committee for Guides in Metrology, 2008). The simulation involves generating random values for variables of interest many times and calculating a result for each set of variables. The results provide a cumulative distribution function that can be used to estimate coverage intervals. A nonparametric bootstrap technique in the R programming language with 100,000 replicates is used for the simulation, as this method does not

require any assumptions about the distribution of the population of the data (Shaw, 2017). At 100,000 replicates, there is convergence to within 0.01 MPa. The assumed "true" (measured) values along with their uncertainties are the inputs to the simulation and are presented in Table 7. "Cal", "hys", and "lin" refer to errors in calibration, hysteresis, and linearity from the manufacturer, respectively. "Rep" is reproducibility error from taking multiple measurements, and "res" is resolution from reading the instrument (half of the smallest digit). Uncertainties in the load cell are from MTS documentation, and dimensional measurement uncertainties are common values expected for Vernier calipers. It is assumed that all random errors and variations in the measurand are all uncorrelated, and that they follow a normal distribution. The results are shown in Table 8. Notably, this uncertainty analysis further expanded the upper and lower bounds of the stress at yield by a larger amount on the smaller samples.

Table 7
Uncertainties used in Monte Carlo simulation.

Measurement	b_{cal}	b_{hys}	b_{lin}	b_{rep}	b_{res}
Force (kN)	0.0075	0.0075	0.0075	0.003	0.001
Width (mm)	0.01	0.01	0.01	0.02	0.005
Thickness (mm)	0.01	0.01	0.01	0.02	0.005

Table 8
Stress at yield results from Monte Carlo uncertainty simulation. Nonparametric bootstrap technique with 100,000 replicates.

Designation	90% Confidence (MPa)	95% Confidence (MPa)	99% Confidence (MPa)
D638-I	22.7 – 24.4	22.5 – 24.6	22.2 – 24.9
D638-II	23.2 – 26.5	22.8 – 26.8	22.3 – 27.4
D638-III	22.7 – 23.9	22.6 – 24.0	22.4 – 24.2
D638-IV	23.3 – 26.7	23.0 – 27.0	22.4 – 27.8
D3039	24.1 – 25.0	24.0 – 25.0	23.9 – 25.2

3.6. Finite Element Analysis Verification

The student edition of the finite element analysis (FEA) software package ABAQUS was used as an exercise in verifying that the empirical model could be used to predict the stress-strain relationship up to the necking regime. ABAQUS presents the ability to determine the nonlinear elastic response of materials by making the following assumptions: the material behavior is elastic, the material behavior is isotropic, the material is incompressible by default, and the simulation will include nonlinear geometric effects. ABAQUS uses a form of the strain energy potential to relate stresses and strains in hyperelastic materials. The most commonly used form of strain energy is the polynomial model (Rivlin and Saunders, 1951), which has a volume dependence and is shown in Eq. 11.

$$U = \sum_{i=j=1}^{N} C_{ij}(\bar{I}_1 - 3)^i(\bar{I}_2 - 3)^j + \sum_{i=1}^{N} \frac{1}{D_i}(J_{el} - 1)^{2i} \tag{11}$$

The value U is strain energy potential, N, C_{ij}, and D_i are material parameters. J_{el} is the elastic volume ratio and $\bar{I}_1$ and $\bar{I}_2$ are the first two strain invariants, which are measures of the material's distortion. C_{ij} material parameters describe the shear behavior and D_i parameters introduce compressibility. ABAQUS is able to accept nominal stress and nominal strain uniaxial tensile test data and perform a least squares fit to determine the material parameters required to create the model. The predicted nominal stress and nominal strain values were input to the FEA for each geometry. A Poisson's ratio of 0.395 was taken from section 3.3 and was used in the simulations to account for biaxial behavior. The dog-bone shaped samples were sectioned to cells where the machine gripped, and two boundary conditions were applied: an encastre condition (all displacements and rotations are zero) on the lower cell and a displacement ramp condition on the upper cell that moved from 0 – 20mm of elongation. A rectangular mesh was used with as many elements as possible, constrained by a maximum number of nodes from the student edition. An example of setting up the D638-I sample is shown in Fig. 20.

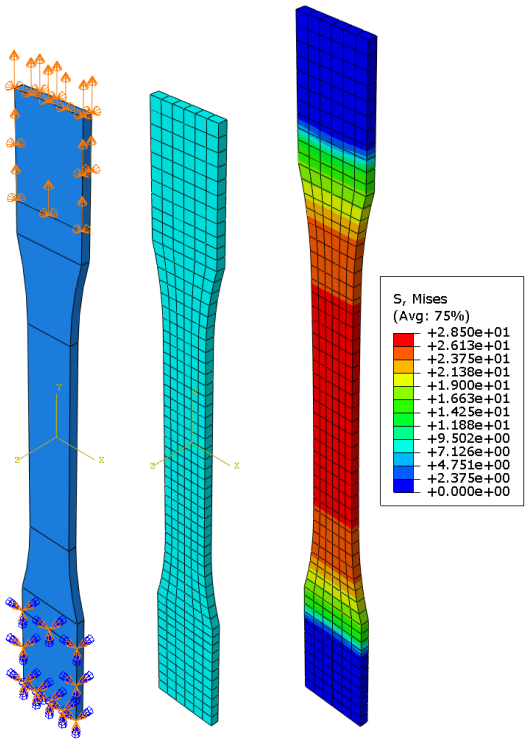

Fig. 20: FEA progression of tensile testing ASTM D638-I specimen. Displays boundary conditions, mesh density, and deflection with von Mises stress result (from left to right).

Since ABAQUS reports the true (von Mises) stress and true strains, those results need to be converted to nominal stresses and strains to compare with the empirical model and to test data. Up to the necking regime, analytical equations can be used to convert to and from nominal and true stresses and strains (Eq. 12 – 13). The empirical model and test data were compared in Fig. 15 – 19, so Fig. 21 – 25 compares the FEA result with the empirical model.

$$\sigma_{true} = \sigma_{nom}(1 + \varepsilon_{true}) \tag{12}$$

$$\varepsilon_{true} = \ln(1 + \varepsilon_{nom}) \tag{13}$$

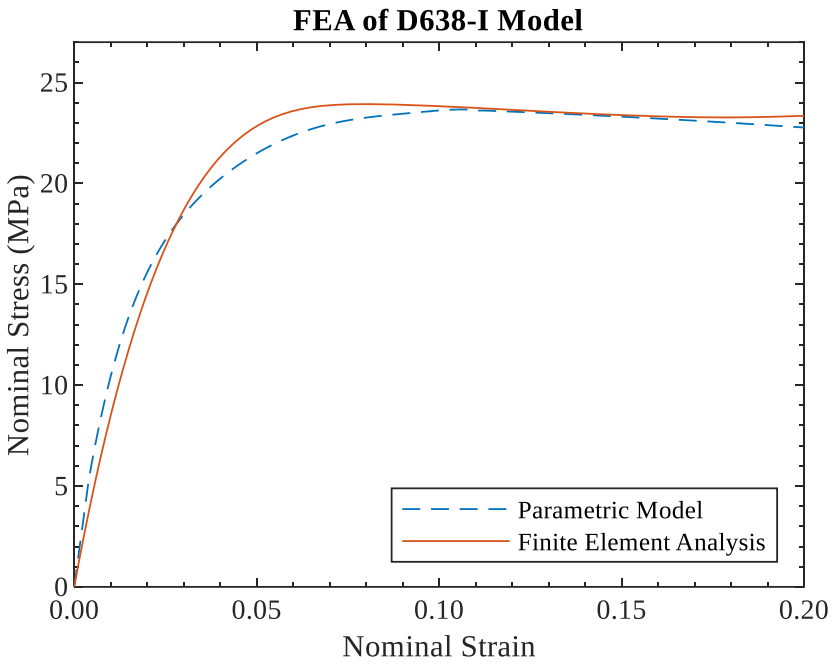

Fig. 21: Comparison of D638-I FEA and Parametric Model.

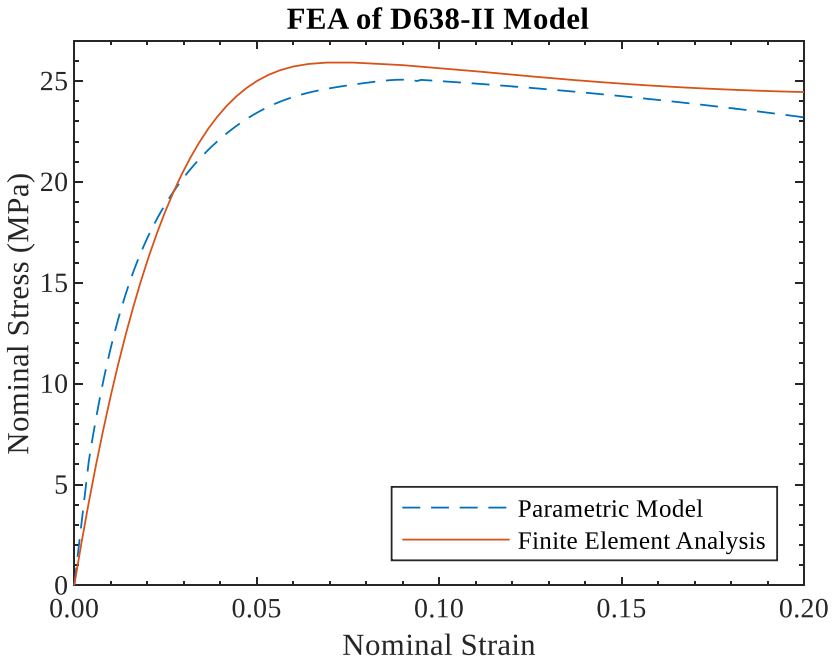

Fig. 22: Comparison of D638-II FEA and Parametric Model.

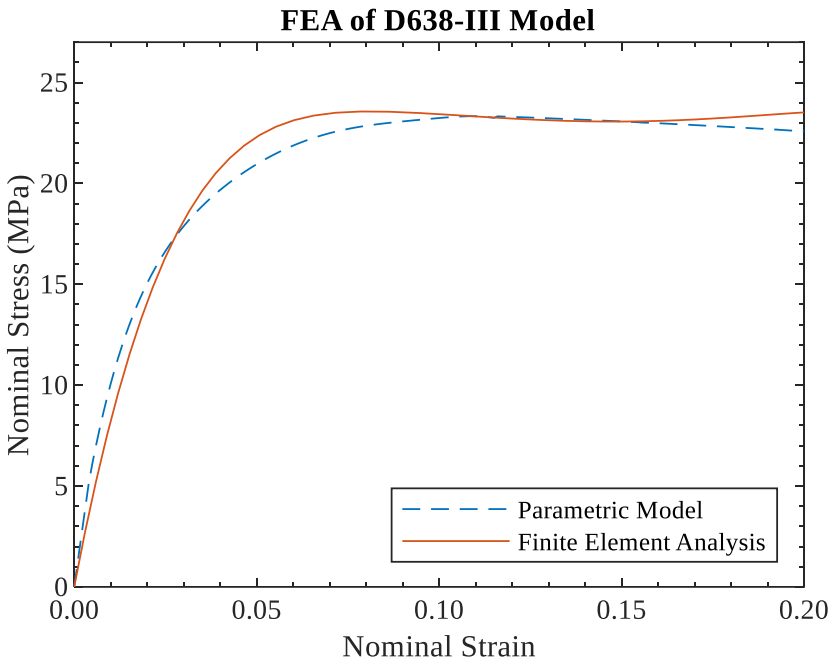

Fig. 23: Comparison of D638-III FEA and Parametric Model.

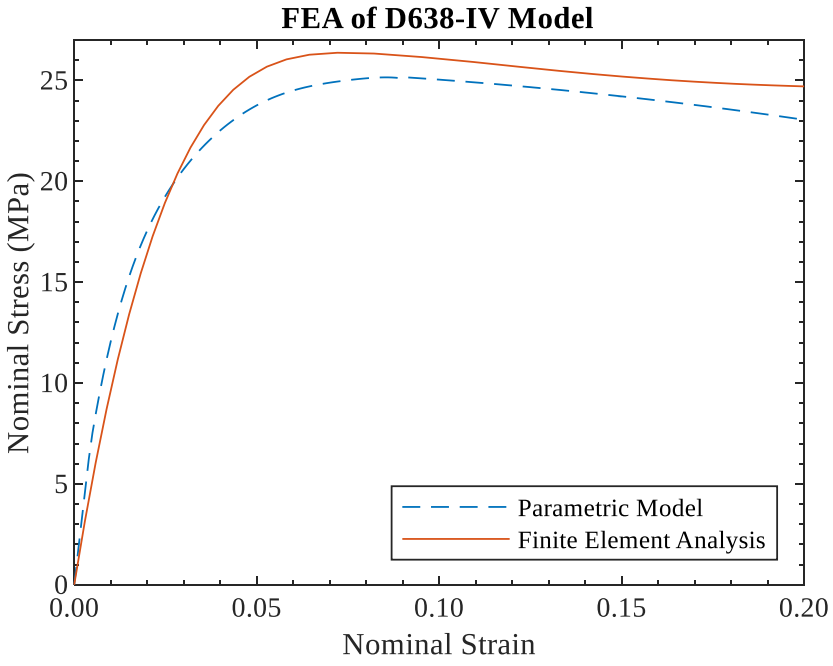

Fig. 24: Comparison of D638-IV FEA and Parametric Model.

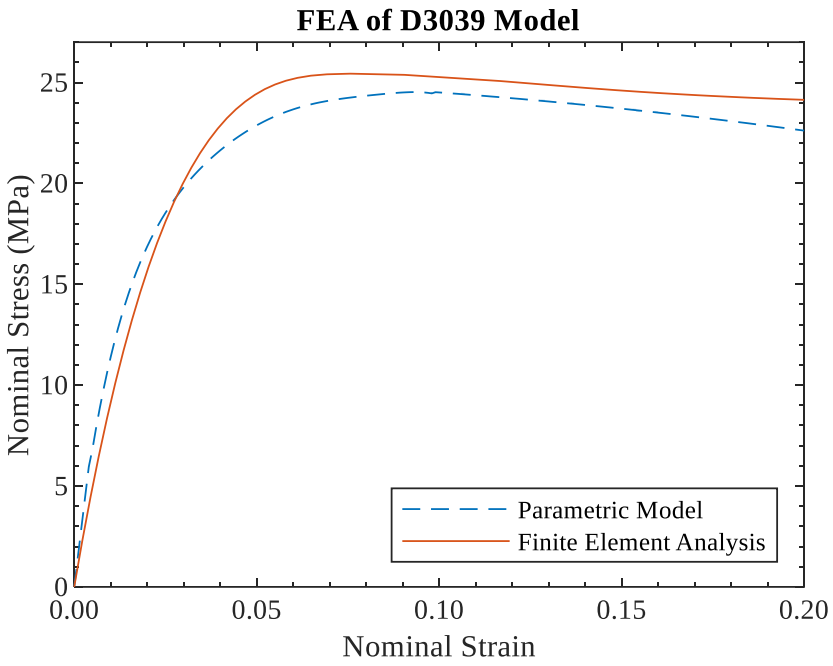

Fig. 25: Comparison of D3039 FEA and Parametric Model.

This finite element analysis serves as a useful tool to generate stress-strain curves at various geometries where stress concentration areas are arbitrary. The FEA-generated stresses can be classified as a conservative model for strains near and after the yield point. One weak point of this analysis is that the only test data passed into ABAQUS was for uniaxial tension tests. The quality of the results from a simulation could be improved by adding test data from planar tension and compression, and equibiaxial tension and compression tests, but those measurements were not taken since complex test machines that can apply those loads have limited availability. However, since uniaxial tension is the mode in which the simulations were run, test data from that strain history is considered adequate. Another important distinction about this FEA model is that it is assumed to be completely

elastic behavior. This is not true in reality since the strain regions modeled in FEA were clearly where the material indicated necking, so using this model to predict unloading is not valid, and doubtful for other strain histories other than uniaxial tension.

A mesh is commonly said to have converged if the desired quantities do not change by more than 5% when refining the mesh. The model database for ASTM D638 Type I used 798 nodes, Type II used 910, Type III used 831, Type IV used 940, and D3039 used 882. In any case, by reducing the number of nodes by one quarter for each, the end result changed by up to 12.2%. Yet, reducing the number of nodes by half changed the end result by up to 3.7%, so the mesh is said to have converged near the maximum number of nodes. Even though the mesh had converged to within 3.7%, being able to use a higher number of nodes for a further convergence study would be of interest.

CHAPTER 4

CONCLUSIONS AND FUTURE WORK

While tensile testing results of HDPE are highly dependent on the testing conditions, the specific specimen size and geometry are also an important factor that one needs to be aware of when scaling-up. The results of this study address how a materials stress-strain response changes as the material's size is scaled-up. For molded, as-machined HDPE in ambient conditions, ASTM D638 Type II is identified as being the most statistically similar to ASTM D3039, with D638 Type IV being similar, but with more scatter. D638 Types I and III acted as conservative estimates for tensile strength at yield and elastic modulus. The empirical model in Section 3.4 of this thesis can be used to predict the geometry-dependent nonlinear stress-strain behavior, which is a required input to hyperelastic finite element structural analysis that was shown to computationally predict material response and vulnerabilities of different geometries. All of the nonlinear deformation before the maximum stress was assumed to be hyperelastic since it is not possible to determine the transition point between nonlinear elastic and plastic deformation with a simple monotonic uniaxial tension test. Future work could involve loading and unloading the material and recording how well it traces the loading path. If there is deviation, the material is not hyperelastic, and even if it does follow the same load path, the assumption of pure hyperelasticity cannot be confirmed with only uniaxial testing. Multiaxial tests

such as planar tension and compression, and equibiaxial tension and compression, while difficult, would provide a definitive determination to the plastic limit and further the validity of parametric and FEA stress-strain response models. The process behind this thesis could be applied to several 3D-printable polymers such as polylactic acid (PLA), for applications in an environment where custom tooling is not readily available, such as aboard the International Space Station. Since this study was concerned with the untreated material tested in ambient conditions, future work could include tests with multifunctional HDPE conditioned with nanoparticles. Additionally, it would be beneficial to have test results for baseline and conditioned HDPE at temperatures representative of a space environment, and increased strain rates that would more accurately represent the actual environmental conditions. In order to obtain more data on Poisson's ratio, the samples would need to be tested at much lower strain rates. It would be increasingly helpful to affix the strain gauges to the samples that follow a wider form-factor. The material may need to be used in space suits, human habitats, and refabrication in space, so there will be a wide variety of strain requirements from structural to semi-structural, and millimeter to meter scales. The range of stresses and strains encompassed in this work provide data for HDPE throughout its operating range, up to and past its maximum strength. The size-scaling effects of this thesis were explored as a first step towards the design of neat polymeric and polymeric multifunctional materials that see potential being incorporated in multidisciplinary space applications.

REFERENCES

ASTM Standard D638 (2014). "Standard Test Method for Tensile Properties of Plastics", ASTM International, West Conshohocken, PA, DOI: 10.1520/D0638-14, www.astm.org.

ASTM Standard D3039 (2017). "Standard Method for Tensile Properties of Polymer Matrix Composite Materials", ASTM International, West Conshohocken, PA, DOI: 10.1520/D3039_D3039M-17, www.astm.org.

ASTM Standard D7565 (2017). "Standard Test Method for Determining Tensile Properties of Fiber Reinforced Polymer Matrix Composites Used for Strengthening of Civil Structures", ASTM International, West Conshohocken, PA. DOI: 10.1520/D7565_D7565M-10R17, www.astm.org.

Carothers, W., Hill, J. (1932). Studies of Polymerization and Ring Formation. XV. Artificial Fibers from Synthetic Linear Condensation Superpolymers. J. Am Chem Soc 1932, 54, 1579-1596.

Chemical Retrieval on the Web (CROW): High-Density Polyethylene. (2019), https://polymerdatabase.com/Commercial%20Polymers/HDPE.html (downloaded in September 2019).

Clausi, M., Toto, E., Botti, S., Laurenzi, S., La Saponara, V., Santonicola, M. G. (2019). "Direct effects of UV irradiation on graphene-based nanocomposite films revealed by electrical resistance tomography", Compos. Sci. and Technol., 183, 107823 (8 pp.), https://doi.org/10.1016/j.compscitech.2019.107823.

Coleman, B. D. (1983). Necking and drawing in polymeric fibers under tension. Arch. Ration. Mech. Analysis 83, 115.

Coleman, H. W. and Steele, W. G. (2009). Experimentation, Validation, and Uncertainty Analysis for Engineers, 3rd ed., Wiley, Hoboken, NJ.

Daver, F. and Cherry, B. W. (1996). Modeling the Elastic Modulus of HDPE in Terms of Stress-Dependent Thermally Activated Rate Process. J. Appl. Polym. Sci., 59, 453-457.

Department of Defense Composite Materials Handbook Military Specification (MIL)-HDBK-17-3F, Volume 3. Polymer Matrix Composites Usage, Design, and Analysis. June 17, 2002, USA.

Dougherty, D.R., and Adams, J.W. (1983). Radiation resistance testing of high-density polyethylene. Brookhaven National Lab, Upton, NY, USA.

Farrell, W. M., Jackson, T. L., Marshall, J. R., and Delory, G. T. (2015). The Need for Conductive Space Suits: A Summary of DREAM2 Findings. Downloaded in September 2019 from https://sservi.nasa.gov/wpcontent/uploads/2015/08/farrell_spacesuit_pdp.pdf

Harrison, C., Waver, S., Bertelsen, C., Burgett, E., Hertel, N., and Grulke, E. (2008). Polyethylene/Boron Nitride Composites for Space Radiation Shielding. J. Appl. Polym. Sci., 109, 2529–2538.

Hutchinson, J.W., Neale, K.W. (1983). Neck propagation. J. Mech. Phys. Solids 31 (5), 405–426.

Jareki, L. and Meier, D. J. (1979). Ultrahigh modulus polyethylene. II. Effect of drawing temperature on void formation and modulus. J. Polym. Sci.: Polymer Phys. Edition, 17, 1611-1621.

Joint Committee for Guides in Metrology 101:2008, Evaluation of measurement data: Supplement 1 to the "Guide to the expression of uncertainty in measurement"—Propagation of distributions using a Monte Carlo method, International Bureau of Weights and Measures (BIPM), Sérres, France, 2008.

Kida, T., Hiejima, Y., and Nitta, K.-H. (2016). Raman Spectroscopic Study of High-density Polyethylene during Tensile Deformation. Int. J. Exp. Spectroscopic Tech. 1:001.

Kreiger, M. A., Mulder, M. L., Glover, A. G., and Pearce, J. M. (2014). Life cycle analysis of distributed recycling of post-consumer high density polyethylene for 3-D printing filament. J. Clean Prod. 70, 90-96.

Laurenzi, S., Santonicola, M. G., Paris, C., De Zanet, G., Rufo, D. (2018). Polyethylene-based Nanocomposites for Radiation Shielding: Modeling in Radiative Environment and Laboratory Tests in Thermo-Vacuum Chamber. Proceedings of the 69th International Astronautical Congress, October 2018, Bremen (Germany).

Lestari, W., Pinto, B., La Saponara, V., Yasui, J., Loh, K. J. (2016) Sensing uniaxial tensile damage in fiber-reinforced polymer composites using electrical resistance tomography. Smart Mater. Struct. 25, 085016 (8pp.).

Milisavljevic, J., Petrovic, E., Ciric, I., Mancic, M., Markovic, D., Dordevic, M. (2012) Tensile Testing for Different Types of Polymers. DAS-29, 29th Danubia-Adria Symposium, University of Belgrade (Serbia).

Narici, L., Casolino, M., Di Fino, L., Larosa, M., Picozza, P., Rizzo, A. and Zaconte, V. (2017). Polyethylene as radiation shielding on-board the International Space Station in high latitude radiation environment. Sci. Rep. 2017, 10;7(1):1644. doi: 10.1038/s41598-017-01707-2.

Neale, K. W. and Tugcu, P. (1985). Analysis of necking and neck propagation in polymeric materials. J. Mech. Phys. Solids 33, 323.

Nitta, K and Yamana, M. (2012). Poisson′s Ratio and Mechanical Nonlinearity Under Tensile Deformation in Crystalline Polymers. Kanazawa University, Kakuma, Kanazawa, Japan. 10.5772/34881.

Ogden, R.W. (1972). Large deformation isotropic elasticity: on the correlation of theory and experimental for compressible rubberlike solids. Proc. Roy. Soc. A-Math. Phy. 328 (157), 567–583.

Orlando, T. M., Jones, B., Paty, C., Schaible, M. J., Reynolds, J. R., First, P. N., Robinson, S. K., La Saponara, V., Beltran, E. (2018). Catalyst: Radiation Effects on Volatiles and Exploration of Asteroids and the Lunar Surface. Chem 4, 8-15.

Prater, T., Werkheiser, N., Ledbetter, F., Jehle, A. (2017). "NASA's In-Space Manufacturing Project: Toward a Multimaterial Fabrication Laboratory for the International Space Station," American Institute of Aeronautics and Astronautics, AIAA SPACE and Astronautics Forum and Exposition, Orlando, FL, https://doi.org/10.2514/6.2017-5277.

Rivlin, R. S. & Saunders, D. W. (1951), 'Large Elastic Deformations of Isotropic Materials. VII. Experiments on the Deformation of Rubber', Philosophical Transactions of the Royal Society A: Mathematical, Physical and Engineering Sciences 243(865), 251–288.

Seibers, Z., Orr, M., Collier, G. S., Henriquez, A., Gabel, M., Shofner, M., La Saponara, V., Reynolds, J. (2019). Chemically Functionalized Reduced Graphene Oxide as Additives in Polyethylene Composites for Space Applications. Polym Eng Sci. doi:10.1002/pen.25262.

Selvadurai, A. (2006), 'Deflections of a rubber membrane', Journal of the Mechanics and Physics of Solids 54(6), 1093–1119.
Semeliss, M. A., Wong, R., Tuttle, M. E. (1990). The Yield and Post-Yield Behavior of High-Density Polyethylene. NASA-Langley Research Center.

Sergueeva, A. V., Zhou, J., Meacham, B.E., and Branagan, D. J. (2009). Gauge Length and Sample Size Effect on Measured Properties during Tensile Testing. Mat. Sci. Eng. A-Struct., 526, pp. 79-83.

Shaw, B. (2017). Uncertainty Analysis of Experimental Data with R. Chapman and Hall CRC Press.

Yeoh, O. H. (1993), 'Some Forms of the Strain Energy Function for Rubber', Rubber Chemistry and Technology 66(5), 754–771.